Catena 182 (2019) 104117

Contents lists available at ScienceDirect

Catena

journal homepage: www.elsevier.com/locate/catena

Inverse relationship between south-west and north-east monsoon during the late Holocene: Geochemical and sedimentological record from Ennamangalam Lake, southern India

Praveen K. Mishra[a,*], Yadav Ankit[b], P.K. Gautam[c,d], Lakshmidevi C.G.[c], Pramod Singh[c], Ambili Anoop[b]

[a] Wadia Institute of Himalayan Geology, 33 GMS Road, Dehradun 248001, Uttarakhand, India
[b] Indian Institute of Science Education and Research Mohali, Manauli, Punjab 140306, India
[c] Department of Earth Sciences, Pondicherry University, Pondicherry 605014, India
[d] Geological Survey of India, Northern Region, Lucknow 226024, India

ARTICLE INFO

Keywords:
North-east and south-west monsoon
Geochemistry
Clay mineralogy
Grain size
End member mixing analysis
Southern India

ABSTRACT

The southern peninsula of the Indian sub-continent is characterized by moisture source from both the south-west (SW) and north-east (NE) monsoon. However, the long-term climate variability associated with these two moisture sources and their relative contribution in the region is less known. In this study, we have used a multiproxy approach (geochemistry, clay mineralogy and end member mixing analyses of the grain size parameters) on the radiocarbon dated sediment profile from Ennamangalam Lake, southern India to reconstruct the past moisture sources in the region. Based on our systematic investigation, we have identified three hydrological stages in the region: stage 1 (ca. 4800 to 3150 cal BP)-relative drier condition, marked by low detrital content, and higher contribution of relatively fine-grained end member (EM) 2; stage 2 (ca. 3150 to 1640 cal BP)-transition phase, high sedimentation rate as compared to the preceding stage; and stage 3 (1640 cal BP to present)-represented by enhanced detrital content, intense chemical weathering (shown by increasing CIA and continuous declining value of Mg/Al) and dominance of EM 1 characterized by coarse grain sediments indicating high energy condition due to the intense precipitation. The regional comparison of paleoclimate records demonstrate that the increase in precipitation observed in Ennamangalam region during the late Holocene is in contrast to the records from the core monsoon zone. The overview of regional records indicate an inverse relationship between the south-west and the north-east monsoon strength during the late Holocene affected by the increasing ENSO variability.

1. Introduction

The agrarian economy and the drinking water requirements of ca. 20% of the world population depend on the Indian monsoon. During the summer season from June to September (JJAS), the moisture in the Indian sub-continent is largely contributed by the south-west (SW) monsoon (also known as Indian summer monsoon or ISM), whereas the zone of maximum rainfall shift to southern India during the north-east monsoon (NEM) season from October to December (OND) (Gadgil, 2006; Kripalani and Kumar, 2004). The NEM provides ~11% of India's annual rainfall and contributes ~17–49% of annual rainfall in southern India (Sreekala et al., 2012). The abrupt changes in the NEM rainfall patterns pose a serious threat to the agricultural output over southern India with a considerable decrease in the crop production observed during the period of below-normal NEM rainfall (Krishna Kumar et al., 2004; Rao Krishna and Jagannathan, 1953). However, in spite of the importance, only limited studies are available on NEM variability (Kripalani and Kumar, 2004; Rajeevan et al., 2012; Sreekala et al., 2012). The available investigation based on modern meteorological data demonstrates that the NEM rainfall shows significant interannual variability with 25% of relative standard deviation (Kripalani and Kumar, 2004; Rajeevan et al., 2012). The correlation analysis of rainfall series for the past 100 years revealed a significant negative correlation between ISM and NEM (Dhar and Rakhecha, 1983). The long-term paleoclimate data from southern India will provide a better understanding of moisture sources and is useful to develop strategies for the seasonal prediction of NEM rainfall in the region which has a strong control over agricultural productivity in the region (Gunnell et al.,

* Corresponding author.
E-mail address: praveenmishra@wihg.res.in (P.K. Mishra).

https://doi.org/10.1016/j.catena.2019.104117
Received 14 July 2018; Received in revised form 7 June 2019; Accepted 9 June 2019
Available online 24 June 2019
0341-8162/

2007).

The majority of terrestrial paleoclimate records from Indian subcontinent have been relied on lacustrine sediments and sedimentary sequences from core monsoon zone (Ponton et al., 2012; Prasad et al., 2014; Sarkar et al., 2015), western India (Laskar et al., 2013; Pillai et al., 2017; Prasad and Enzel, 2006 and references therein) and NW Himalayan region (Anoop et al., 2013a; Leipe et al., 2014; Mishra et al., 2015; Rawat et al., 2015; Sanwal et al., 2013; Srivastava et al., 2017; Wünnemann et al., 2010) to understand the long-term climate variability of ISM precipitation. In contrast, only a few paleoclimate records are available from southern India- the region influenced by both ISM and NEM precipitation (Basu et al., 2017; Rajmanickam et al., 2017; Sandeep et al., 2017; Shetty et al., 2018; Sukumar et al., 1993; Veena et al., 2014). These investigations have mostly interpreted the paleoclimate dataset in terms of variability in ISM precipitation alone (Sandeep et al., 2017; Sukumar et al., 1993; Veena et al., 2014) and no attempts have been made to disentangle the contributions of ISM and NEM in the region.

In this study, we present a multiproxy approach integrating geochemistry, clay mineralogy and end member mixing analyses (EMMA) on grain size parameters from a sedimentary profile in Ennamangalam Lake, southern India spanning over the last ~4800 cal BP in order to: (i) understand the temporal variability in sedimentological and geochemical characteristics; (ii) identify any hydrological changes associated with the changes in the ISM or NEM precipitation during the late Holocene; and (iii) understand the possible drivers of the precipitation changes via regional comparisons of paleoclimate data.

2. Study area

2.1. Geographic setting

The Ennamangalam Lake (11.65°N, 77.59°E, and ~265 masl) is located at the foothills of Biligirirangan Hills (BR Hills) in Erode district, Tamil Nadu (southern India) (Fig. 1a–b). The circular lake has a surface area of ~1.54 km^2 with a maximum extension of ~0.7 km in NS and ~0.8 km in EW direction (Fig. 1c). Geologically, the region forms a part of Southern Granulite Province with the lake catchment comprising of Al, Fe rich-charnockites, hornblende-biotite gneiss and granites (Kavidha and Elangovan, 2012; Nanthakumar et al., 2010; Ray et al., 2003; Samuel et al., 2018). The lake is mostly fed by the ephemeral streams from the southern slope of the BR hills active during the monsoonal period. Additionally, a small spring visible during the non-monsoonal period (January to May) located in the western part of the lake basin also supplement the lake water budget.

2.2. Modern climate

The Ennamangalam Lake, situated at the transition zone between ISM and NEM region, provides an ideal location to reconstruct the past moisture condition in southern India. Based on the average annual precipitation data (2005–2016 CE) recorded from the nearest meteorological station in Erode district (11°29′N and 77°46′E), the region receives ~728 mm of rainfall annually with ~33% of rainfall contributed from ISM (JJAS) and ~46% during the NEM (OND) (source: Indian Meteorological Department) (Fig. 1d). To understand the dominant moisture source in the region, isentropic back trajectory ensembles for Erode district have been plotted using HYSPLIT model provided by National Oceanographic and Atmospheric Administration (NOAA) and Air Resources Laboratory (ARL) (Breitenbach et al., 2010; Mishra et al., 2018b; Sinha et al., 2015) for the year 2012 CE. The back trajectory analysis shows that the monsoonal winds bring moisture from the Arabian Sea (during JJAS), whereas Bay of Bengal is the key source of moisture in the study area during OND (Fig. 1e). The local average temperature in Erode district varies between ~39 °C to 24 °C during the summer and ~32 °C to 20.5 °C during the winter (Rajkumar et al., 2010).

3. Methodology

3.1. Field sampling

During the field expedition in May–June 2012 CE (premonsoon season), sediment samples were collected from 165 cm deep trench excavated within the dried out lake basin (Figs. 1c, d and 2a). The sediments from the vertical profile are sampled at 5 cm resolution. The geochemical and clay mineralogical analysis of the Ennamangalam Lake profile was conducted at the Department of Earth Sciences, Pondicherry University (India), whereas the grain size analyses were performed at the Wadia Institute of Himalayan Geology, Dehradun (India).

3.2. Analytical methods

3.2.1. Chronology

The chronology of the Ennamangalam Lake profile is based on four accelerator mass spectrometry (AMS) ^{14}C dates of bulk organic sediments. The detailed description of the chronology reconstruction has been previously discussed in Basu et al., 2017. The radiocarbon age was calibrated using the online version of OxCal 4.1 software (Ramsey et al., 2010; Reimer et al., 2013). The calibrated ages are represented as cal BP with ± 1 standard deviation (Table 1).

3.2.2. Geochemical analysis

About ~50 g of oven dried and homogenized samples were powdered to a mesh size of 75 μm (sieve designation-200) using a planetary ball mill. The powdered samples were subsequently digested following the conventional acid-digestion procedure (Shapiro and Brannock, 1962) using HF-HNO_3-HCl acids in the closed Teflon beakers on a hotplate at 120 °C. Quantitative analysis was conducted using inductively coupled plasma atomic emission spectroscopy (ICP-AES, Horiba Jobin Yvon Ultima 2). The instrument was calibrated against USGS rock standards BHV0-1, STM-1, RGM-1 and laboratory standards VM-9, 21-6, 22-22 and 22-7. The precision of the major element analysis is better than 2%.

3.2.3. Clay mineralogy

The clay mineral fraction (< 2 μm) used for XRD analysis was separated by settling method according to Hardy and Tucker, 1988. The air-dried samples were first treated with 5 ml of hydrogen peroxide (30% H_2O_2) to remove organic materials, which was then thoroughly washed with distilled water. Furthermore, the sample suspended in the settling column was mixed with 10 ml of Calgon (Sodium Hexa metaphosphate) to de-flocculate clay minerals. The oriented clay samples for X-ray diffraction (XRD) were prepared by carefully pipetting the clay suspension onto a glass slide.

Clay mineral was analyzed using a PANalytical XPert Pro™ X-Ray Diffractometer (XRD) equipped with a copper target, operating at 40 kV and 25 mA. XRD patterns of oriented clay slides were recorded using a step size of 0.02° 2θ with a scan speed of 0.6° 2θ/min and scanned from 2° to 40° 2θ. The semi-quantitative estimates of clay minerals were determined using peak areas of smectite (15–17 Å), illite (10 Å), and kaolinite (7 Å). The peak areas of the spectra of these clay minerals were calculated using the glycolated X-ray diffractograms and relative weight percentages were calculated following the semi-quantitative method outlined in Biscaye, 1965.

3.2.4. Grain size analysis

The grain size distribution of the Ennamangalam Lake sediment was

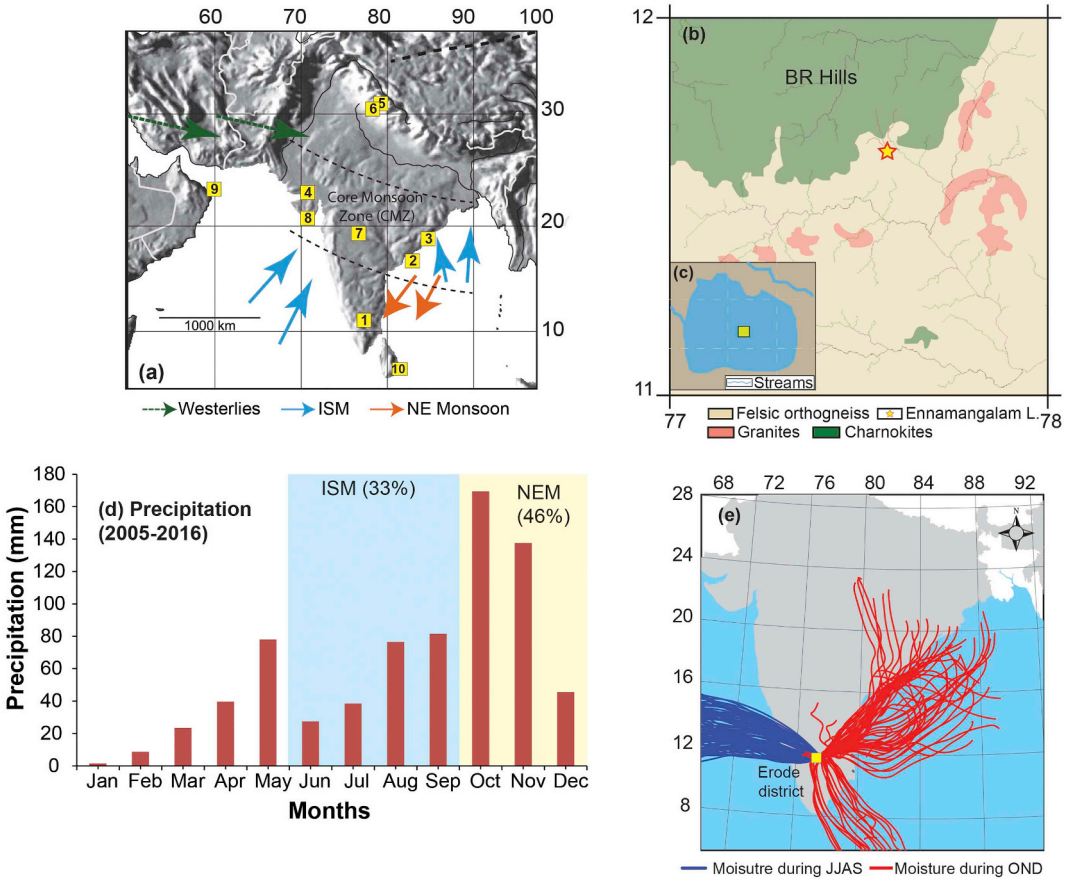

Fig. 1. (a) Physiographic map of Indian sub-continent with dominant wind patterns in the study area and approximate limits of core monsoon zone indicated by the dotted lines (modified from Rajeevan et al., 2010). Paleoclimate sites discussed in the text are marked by numbers - (1) This study, (2) Ponton et al. (2012), (3) Ankit et al. (2017), (4) Pillai et al. (2017), (5) Mishra et al. (2015), (6) Rawat et al. (2015), (7) Prasad et al. (2014), (8) Banerji et al. (2015), (9) Gaye et al. (2017), (10) Ranasinghe et al. (2013); (b) the geological map of the region (modified after Samuel et al., 2018), 'star' represent the location of Ennamangalam Lake; (c) detailed image of the lake basin (yellow square showing the location of sediment profile); (d) seasonal precipitation in the Erode district during 2005–2016 CE; (e) air mass trajectory in the study area during SW (blue) and NE (red) monsoon condition in Erode district during the year 2012. (For interpretation of the references to colour in this figure legend, the reader is referred to the web version of this article.)

measured using Malvern Mastersizer 2000E. Total 26 samples have been analyzed representing ~180 years (per sample) of temporal resolution. The pre-treatment of the samples (~0.3 g) included wet oxidation of organic matter at room temperature using 10 ml H_2O_2 (30%) and removal of authigenic carbonates by 5 ml of HCl (0.5 N). Furthermore, the treated samples were washed with distilled water and centrifuged 4–5 times to remove the extra oxidizing agent. To prepare a homogenous solution for the analysis the particle aggregates were disintegrated by handshaking combined with ultrasonic bath.

The instrument measured the grain-size distribution of the suspended particles from 0.02 to 2000 μm for 100 grain-size classes. The average value from the multiple measurements (n = 5) of each sample has been used to represent the grain size distribution.

3.3. Data analysis

3.3.1. End member mixing analysis (EMMA) of the grain size distribution

End member mixing analysis (EMMA) is a statistical approach to unmix grain size distributions into meaningful subpopulations that represent grain size sorting, transport and depositional processes (Dietze et al., 2012; Weltje, 1997). The end member mixing analysis was performed using R-script (package: *EMMAgeo; version-0.9.2*) based algorithm (Dietze et al., 2014, 2012). For EMMA, the grain size dataset was rescaled to the constant values after removal of zero or blank (or NA) values (Dietze et al., 2012; Li and Li, 2017; Weltje, 1997). The relation between end members (q) (varies between q_{min} and q_{max}) and quantile range (between 0 and l_{max}) define the infinite number of end member models (Dietze et al., 2013). The l_{max} is defined as the highest possible quantile allowing numerically stable weight transformations (Dietze et al., 2014; Miesch, 1976). Furthermore, the robust end members were calculated based on the high frequency of non-overlapping modes of similar end member loadings in adjacent grain size classes (Dietze et al., 2014). The output provided by EMMA mainly consisted of (i) loadings, characterized by typical grain size distribution related to distinct sorting of sediments from different source and depositional processes, and (ii) scores, represent the down-core variation of the grain size in terms of contribution of end members in each samples (Borchers et al., 2016; Dietze et al., 2013, 2012).

4. Results

4.1. Chronology and sedimentation rate

Based on the colour and textural variability, the Ennamangalam sedimentary profile was divided into three litho-units. The lower part (165–110 cm) of the profile consists of dark grey clay overlained by

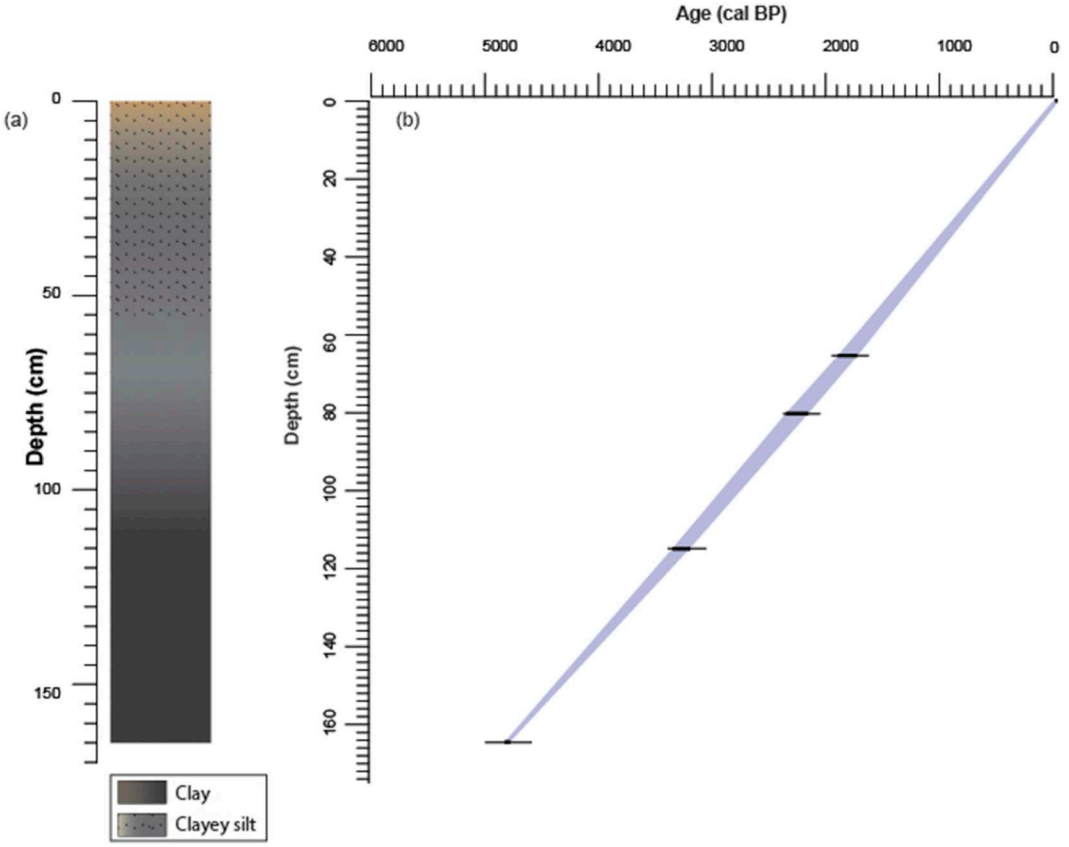

Fig. 2. (a) Detailed litholog of Ennamangalam Lake sediment; (b) the reconstructed chronology of the Ennamangalam lake sediments based on the OxCal 4.1 calibration program.
(Adopted from Basu et al. (2017).)

Table 1
Radiocarbon ages of the core sediments based on OxCal calibration (Ramsey et al., 2010; Reimer et al., 2013).

Lab name	^{14}C year BP	Calibrated age (cal BP) ± 1σ	Depth (cm)
Surface	–	−62	0
ULA-5515	1850 ± 20	1782 ± 36	65
ULA-5388	2235 ± 25	2235 ± 51	80
ULA-5387	3065 ± 20	3284 ± 39	115
ULA-5386	4285 ± 25	4851 ± 16	165

light grey clay sediments (110–60 cm). The sediments from 60 to 0 cm are characterized by clayey silt sediments (Fig. 2a). The chronology of the Ennamangalam sediment sequence has been provided in Table 1 and the age-depth model is shown in Fig. 2b. The presence of non-carbonates rocks in the catchment eliminates the possible contamination by old carbon (Anoop et al., 2013a; Hou et al., 2012; Mischke et al., 2013). Hence, the reservoir correction has not been employed while reconstructing the chronology. The reconstructed chronology of the Ennamangalam sediment sequence covers last ~4800 cal BP.

4.2. Geochemistry

4.2.1. Interrelation between the elemental data

In Ennamangalam sediment sequence, Al_2O_3, FeO and SiO_2 show the dominant contribution in the sediments. The concentration of Al_2O_3 varies between 12.5 and 15.7% (average = 14 ± 0.9%), with maximum values during ca. 3150 and 1640 cal BP. Similarly, FeO shows a continuous increasing trend from ~4800 cal BP to present with highest values around ~1070 cal BP (7.6%) (Fig. 3). However, the SiO_2 concentration ranges between 69 and 75% with maximum contribution during ~4800 to ~3150 cal BP.

Table 2 shows the correlation of major oxides in Lake Ennamangalam. The TiO_2 shows a significant correlation with MnO_2, whereas poor relation with other detrital elements such as FeO and Al_2O_3. However, FeO is highly correlated with Al_2O_3 ($r = 0.65$; $p < 0.01$) signifying a representative of detrital input into the lake. In addition, the strong positive correlation between CaO and Sr ($r = 0.88$; $p < 0.01$) and their poor relation with Al_2O_3 indicates a non-silicate source of CaO and Sr.

4.3. Clay mineralogy

The major clay minerals detected in the Ennamangalam Lake sediments include illite, kaolinite and smectite. The general trend of clay assemblage shows a relatively low concentration of kaolinite (8–19%; except in two samples) in all the three stages, whereas considerable variation has been observed in smectite and illite. Illite ranges between 10.7 and 65.4% of total clay content and has the highest concentration during ~4800 to 3150 cal BP whereas, smectite (~21.4 to 71.4% of the total clay) shows the highest concentration from ~3150 to present.

4.4. Grain size

The particle size distribution of lake sediments show unimodal

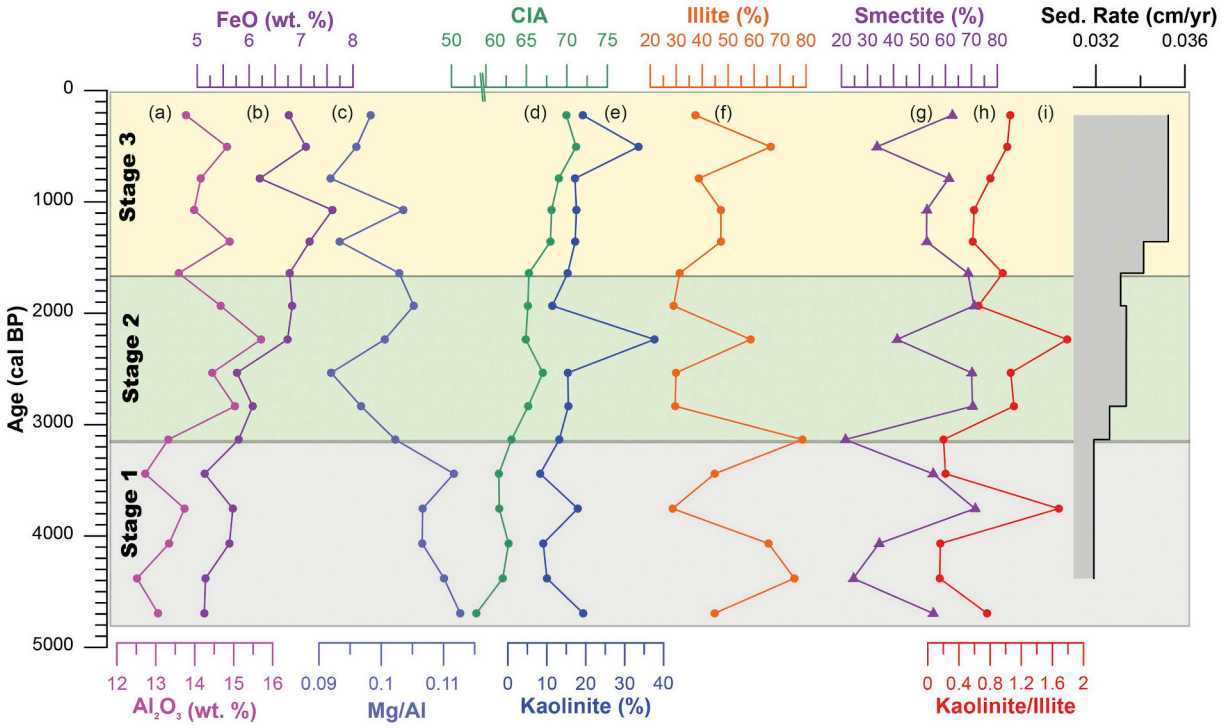

Fig. 3. The geochemical parameters (a–d), clay mineralogy (e–h) and sedimentation rate (i) of the Ennamangalam sediment profile.

Table 2
Correlation matrix between the element oxides.

	SiO_2	TiO_2	Al_2O_3	FeO	MgO	MnO_2	CaO	Na_2O	K_2O
SiO_2	1.00								
TiO_2	−0.44	1.00							
Al_2O_3	**−0.77***	0.18	1.00						
FeO	−0.52	0.26	**0.65**	1.00					
MgO	**−0.70**	0.58	0.37	0.17	1.00				
MnO_2	−0.32	**0.68****	0.14	−0.24	0.60	1.00			
CaO	−0.27	0.42	−0.02	−0.54	**0.65**	**0.80**	1.00		
Na_2O	−0.15	0.39	−0.39	−0.54	0.36	0.47	**0.66**	1.00	
K_2O	−0.28	−0.05	−0.30	−0.45	0.25	0.12	0.41	**0.74**	1.00

The bold values are significantly positive and negative values. The description has been already been there in the main text.

* Significant negative correlation.

** Significant positive correlation

distribution and is largely characterized by clayey silt (Fig. 4a–b). In Ennamangalam sediment profile, three probable number of end members have been identified which explain ~63% of the total variance in the dataset (Fig. 4c). EM 1 with a total measured variance of 20% shows a dominant mode (5 ϕ) in medium-silt size fraction, whereas EM 2 (variance = ~38%) explains the dominant mode of 7 ϕ in fine-silt size fraction. The EM 3 with a variance of ~42% shows a bimodal distribution with a primary mode at 9 ϕ (clay sized fraction) (Fig. 4c).

5. Discussions

5.1. Climate interpretation from the multiproxy approach

The multiproxy record of Ennamangalam sediment profile is shown in Fig. 3. Based on the colour and textural variability (Section 4.1), and sedimentation rate, the sediment sequence can be divided into three stages: stage 1: ~4800 to 3150 cal BP; stage 2: ~3150 to 1640 cal BP and stage 3:~1640 cal BP to present. These stages can be interpreted in terms of hydrological changes in the region and the details of each proxy are discussed below:

5.1.1. Geochemical proxies

The use of Pearson correlation coefficient and principal component analysis (PCA) (Supplementary material S1) to measure the relationship between two or more variables (El-nady and Lotfy, 2016; Koinig et al., 2003; Pulice et al., 2013; Xue et al., 2011) have been utilized in the evaluation of geochemical dataset from Ennamangalam sediments. In Ennamangalam Lake sediments, based on the correlation matrix between different oxides, it is evident that FeO and Al_2O_3 are representative of detrital contribution from the catchment and can be used as a proxy for the surficial runoff. As discussed earlier (Section 2.1), the catchment of Ennamangalam Lake comprises of charnockites, biotite gneiss and granite which are the key source of Na_2O, K_2O, FeO and Al_2O_3 in the sediments (Fig. 1b). The detrital element (Al_2O_3, FeO) shows an increasing concentration from stage 1 to 3 in the sediment sequence (Fig. 3) suggesting an increase in the surface runoff associated with enhanced precipitation.

The presence of calcium (although very low concentration) in the sediment profile (2 to 3%) indicates two possibilities i.e. (i) either detritus from the catchment contributes CaO through surface runoff, or (ii) authigenic precipitation within the lake due to the evaporation process (Leng et al., 2010; Mishra et al., 2015; Talbot, 1990). Relatively higher concentration of CaO (2.0% to 3%) in sediments as compared to Na_2O (0.78% to 1.3%) suggested an additional source for CaO than silicate fraction. Therefore, in absence of carbonate rocks in the catchments, the CaO value indicates endogenic precipitation of the carbonates. The high summer temperature in the region could be the possible reason for evaporation of the residual water content within the lake basin resulting in the precipitation of endogenic CaO.

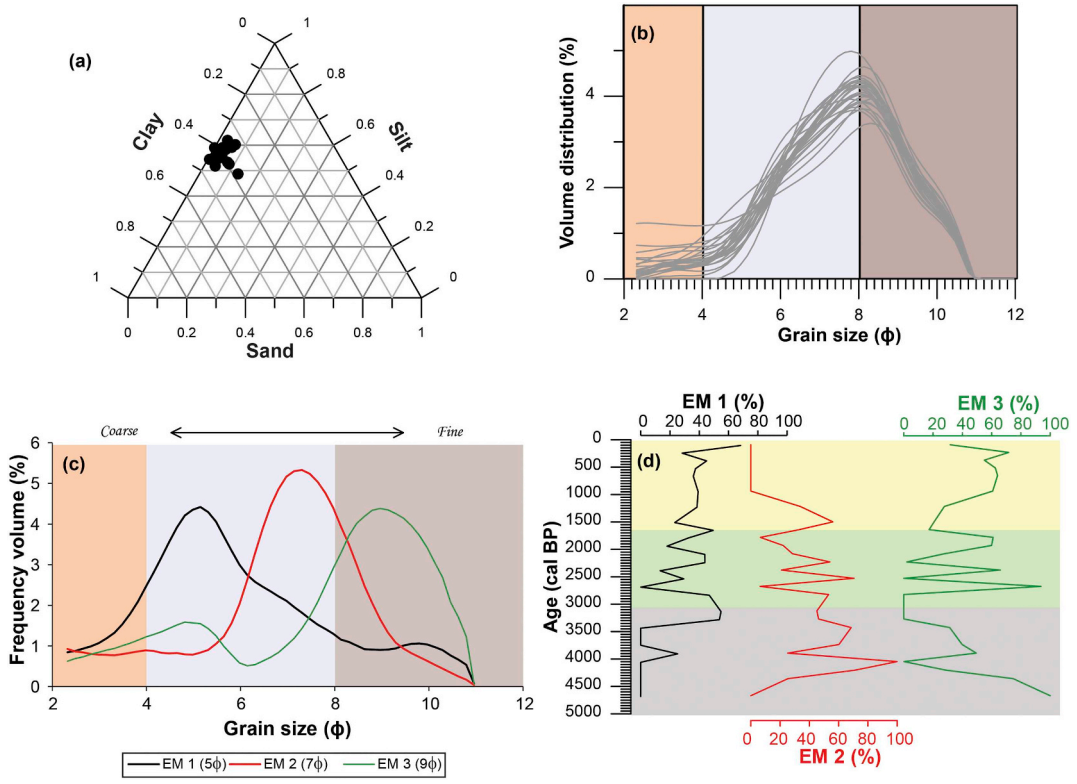

Fig. 4. Grain size distribution in Ennamangalam lake sediment: (a) ternary plot of relative contribution of grain size; (b) volume distribution of samples from the lake profile; (c) frequency distribution of end member loadings (dominant modes in brackets); and (d) temporal variability of three EMs.

5.1.2. Weathering indices

The element ratios and indices derived from major element geochemistry have been used to infer precipitation induced chemical weathering in the Ennamangalam basin. The elemental ratios and indices are widely applied to infer the intensity of catchment weathering, changes in provenance and hydrodynamics processes in the catchments (Buggle et al., 2011; Lopez et al., 2006; Opitz et al., 2015; Railsback, 1993; Singer, 1980). The relation between mobile versus immobile element is the key principle to investigate the weathering indices (Limmer et al., 2012). During the weathering process, the parent material is depleted in mobile elements and enriched in the immobile elements (Buggle et al., 2011).

5.1.2.1. Mg/Al:. The major oxides such as CaO, MgO, and Na_2O are usually soluble and mobile, whereas Al_2O_3, SiO_2, and TiO_2 are considered more insoluble and resistant during chemical weathering (Buggle et al., 2011; Engstrom and Wright, 1984; Girone et al., 2013; Minyuk et al., 2013). The catchment of Ennamangalam Lake is characterized by high Mg containing rocks (Charnockites massifs) which are prone to chemical weathering (Peucat et al., 1989). In Ennamangalam sediment profile, the Mg/Al values decreased from stage 1 to 3 (0.11 to 0.09) (Fig. 3). As Mg is more prone to chemical weathering as compared to Al which is conservative and resistant to weathering in nature, the decreasing values of Mg/Al can be used to trace past weathering condition in the basin (Limmer et al., 2012; Zhong et al., 2012). The decreasing Mg/Al value from stage 1 to 3 indicates increasing chemical weathering in response to an increase in precipitation in the region.

5.1.2.2. Chemical index of alteration (CIA):. The CIA is expressed as molar volumes of $[Al_2O_3 / (Al_2O_3 + CaO^* + Na_2O + K_2O)] \times 100$, where CaO* represent abundance of CaO in silicate fraction, and exclude CaO combined in carbonates and phosphates minerals (Fedo et al., 1995; Gioia et al., 2011; Nesbitt and Young, 1989). The molar ratio of CaO/Na_2O as proposed by McLennan et al. (1993) has been used to calculate CaO*. The index has been widely used as an indicator for plagioclase weathering intensity (Fedo et al., 1995; Hofer et al., 2013; Nesbitt and Young, 1989; Opitz et al., 2015). The CIA values below 50 are considered as un-weathered samples, however, the increased value (> 50 up to 100) indicates a progressive increase in the intensity of weathering with the removal of alkali and alkaline earth elements (Fedo et al., 1995; Nesbitt and Young, 1989). The increasing CIA values from stage 1 to 3 indicate a progressive increase in chemical weathering during the late Holocene (Fig. 3). The result is also corroborated by decreasing Mg/Al ratio (Fig. 3) suggesting enhanced chemical weathering from stage 1 to 3.

5.1.3. Clay mineralogy

Clay minerals are widely used to document and resolve a wide spectrum of depositional environment and their link with the changing climatic conditions (Alizai et al., 2012; Brown and Brindley, 1980; Keller, 1970; Środoń, 1999). The clay mineral assemblages are mainly governed by climatic condition, rock composition (Alizai et al., 2012; Fagel and Boës, 2008; Odoma et al., 2013; Singer, 1980; Thamban et al., 2002) and tectonic activity (Liu et al., 2007). However, the clay mineral zonation in the continental settings mostly indicates climate as the primary factor for controlling the clay mineral distribution (Fagel and Boës, 2008; Galán, 2016; Yuretich et al., 1999). The Ennamangalam sediment sequence is characterized by three clay minerals i.e. illite, smectite, and kaolinite. The presence of illite represents the extent of physical erosion (in arid to semi-arid environment), smectite in the sediments are usually related to chemical weathering, whereas the kaolinite mineral formation indicates prevalence of warm and humid climate (Nagasundaram et al., 2013; Odoma et al., 2013; Singer, 1980; Thamban et al., 2002). In Ennamangalam sediments, the increasing kaolinite and smectite content from stage 1 to 3 indicates

increased chemical weathering in the basin due to high moisture availability (Fig. 3). The enhanced weathering of plagioclase and mafic minerals (pyroxene, hornblende and biotite) in the catchment rocks resulted in increased kaolinite and smectite concentration respectively from stage 1 to 3. This inference is also supported by progressively increasing (decreasing) CIA (Mg/Al) trend (Fig. 3). Additionally, clay mineral ratios also provide information on the paleoenvironmental changes with increasing Kaolinite/Illite ratio corresponds to warm/humid condition (Alizai et al., 2012; Churchman, 2000; Odoma et al., 2013). Although a few samples show high values (e.g., in stage 1 and 2) (Fig. 3), the overall increasing trend for Kaolinite/Illite ratio indicates the prevalence of more humid conditions during the later part of the late Holocene.

5.1.4. Grain size

Grain size fluctuation in the lake sediments mostly reflects (i) energy and mode of transport in the lake basin; and (ii) shoreline proximity (Basavaiah et al., 2014; Cuven et al., 2010; Vandenberghe et al., 1997). The end member mixing analysis provides an effective tool to un-mix the grain size distribution based on various depositional environments (Borchers et al., 2016; Dietze et al., 2012; Vandenberghe et al., 1997). The end-member analyses have been successfully applied in various terrestrial (Borchers et al., 2016; Dietze et al., 2012; Li and Li, 2017) and marine sediments (Beuscher et al., 2017; Hamann et al., 2008) to disentangle the different transport processes (fluvial, aeolian and glacial).

In Ennamangalam Lake, the end member 1 (mode = 5 ϕ) and 2 (mode = 7 ϕ) lies in the range of medium and fine silt respectively. The end member modeling analyses from the Tibetan lakes and catchments suggested that this grain size fractions were associated with local and regional dust particle characterized by aeolian deposits (Dietze et al., 2014). However, the role of aeolian processes in the relatively more humid region and vegetation covered Ennamangalam region is very limited. Thus, EM1 and EM2 in Ennamangalam Lake sediments represent the fluvial sediment component transported to the basin.

The coarse end member (EM) 1 grain sizes are deposited by high-energy fluvial transport during the period of enhanced surficial runoff (Anoop et al., 2013a). Additionally, the anthropogenic induced erosion in the catchment could also contribute to increase in terrigenous sediments into the basin (Bhattacharya and Byrne, 2016; Issaka and Ashraf, 2017). The increasing trend of EM 1 (since ca. 4800 cal BP) demonstrates the gradual increase in the energy condition in the surface runoff due to the intense precipitation (Fig. 4d). This interpretation is corroborated by geochemical values showing increased chemical weathering due to enhanced precipitation during the late Holocene (Figs. 3 and 4d). Likewise, the decreasing trend of EM 2 (represented by fine silt size fraction) demonstrates deposition of relatively finer fraction during the period of relatively low energy condition (stage 1 and 2). The EM 3 having a primary mode in the range of clay-sized fraction shows fluctuating values with absence of any specific trend as well as relation with geochemical parameters. The relative changes in the EM1 and EM2 contribution leads to the fluctuation in EM3 suggesting that, in times of reduced fluvial silt deposition, clays could deposit at the basin centre.

5.2. Climate variability in the region

5.2.1. Regional comparison of paleoclimate data

Based on the multiproxy approach, the paleoclimatic record from Ennamangalam Lake demonstrates a progressively increasing trend of precipitation from ~4800 cal BP to present (Fig. 5a). However, several well-dated records from the core monsoon zone (CMZ) suggest increased aridity during the beginning of late Holocene associated with a weakening of the south-west monsoon winds (Anoop et al., 2013b; Ponton et al., 2012; Prasad et al., 2014) (Fig. 5b). Geochemical record from eastern India also reveals increased precipitation between 4800 and 3100 cal BP followed by a reduction in monsoonal strength towards the present (Ankit et al., 2017) (Fig. 5c). A recent multi-proxy study from the semi-arid region of Saurashtra coast in north-west India also suggests the presence of relatively humid climate and higher sea-level between 4710 and 2825 cal BP followed by a gradual onset of aridity between 2825 and 1835 cal BP (Banerji et al., 2015). Additionally, the paleorecord based on oxygen isotopic composition of gastropod shell from western India also demonstrated decreasing ISM precipitation during the late Holocene (Pillai et al., 2017) (Fig. 5d). Studies based on geochemistry, palynology and $\delta^{18}O_{carb}$ values from western and north-west Himalayas also show a progressive decrease in ISM intensity and (I/E) ratios ([meltwater + monsoon precipitation] / evaporation) during the mid-late Holocene following the declining in the solar insolation curve (Demske et al., 2009; Mishra et al., 2018a; Rawat et al., 2015) (Fig. 5e). In contrast, the multiproxy record from Ennamangalam Lake demonstrates enhanced precipitation in the region during the late Holocene contrary to the paleoclimate data derived from the regions dominated by ISM precipitation. The increased precipitation during late Holocene observed in Ennamangalam region can therefore only be explained in terms of strengthening of NE monsoon precipitation in the region (Fig. 5a). This strengthening of NE monsoon during the late Holocene is in line with $\delta^{15}N$ records from the Arabian Sea sediments (Gaye et al., 2017). The paleoclimate record from the Panama estuary (Sri Lanka) also shows an intensified winter monsoon during the mid-late Holocene with a short interval of arid phase (Ranasinghe et al., 2013). However, several other records from NE monsoon dominated regions in Sri Lanka shows a similarity with the climate record from the ISM in India (Ranasinghe et al., 2013), and explained these in terms of common forcing mechanisms.

5.2.2. Factors promoting an increase in the NEM strength during late Holocene

In a recent global warming scenario, the increasing NEM rainfall in peninsular India is positively correlated to various teleconnections such as El-Nino Southern Oscillations (ENSO) and India ocean dipole mode (IODM) (Dhar and Rakhecha, 1983; George et al., 2011; Kripalani and Kumar, 2004; Yadav, 2012). During the El-Nino years, the warming of sea surface temperature (SST) over the equatorial Indian Ocean induces deep convection, resulting in increased NE monsoon precipitation over southern India (Yadav, 2012). Additionally, the anomalously warm SSTs in the western Indian Ocean during IOD and the associated large-scale convergence extending towards the south of India also leads to intensified NEM rainfall (Kripalani and Kumar, 2004). The sedimentation record in Laguna Pallcacocha, southern Ecuador, which is strongly influenced by ENSO variability demonstrate increasing ENSO events during the late Holocene (Moy et al., 2002) (Fig. 5f). This increasing ENSO variability during late Holocene resulted in the significant decline of the ISM precipitation in CMZ (Prasad et al., 2014). We assume that the increasing ENSO events and sea surface temperature over the equatorial Indian Ocean during the late Holocene resulted in reduction of the ISM precipitation in CMZ, which allowed a strengthening of NE monsoon during the same time period. However, additional paleorecords from the NE monsoon domain is required to further evaluate the physical mechanism controlling the moisture contribution in the region.

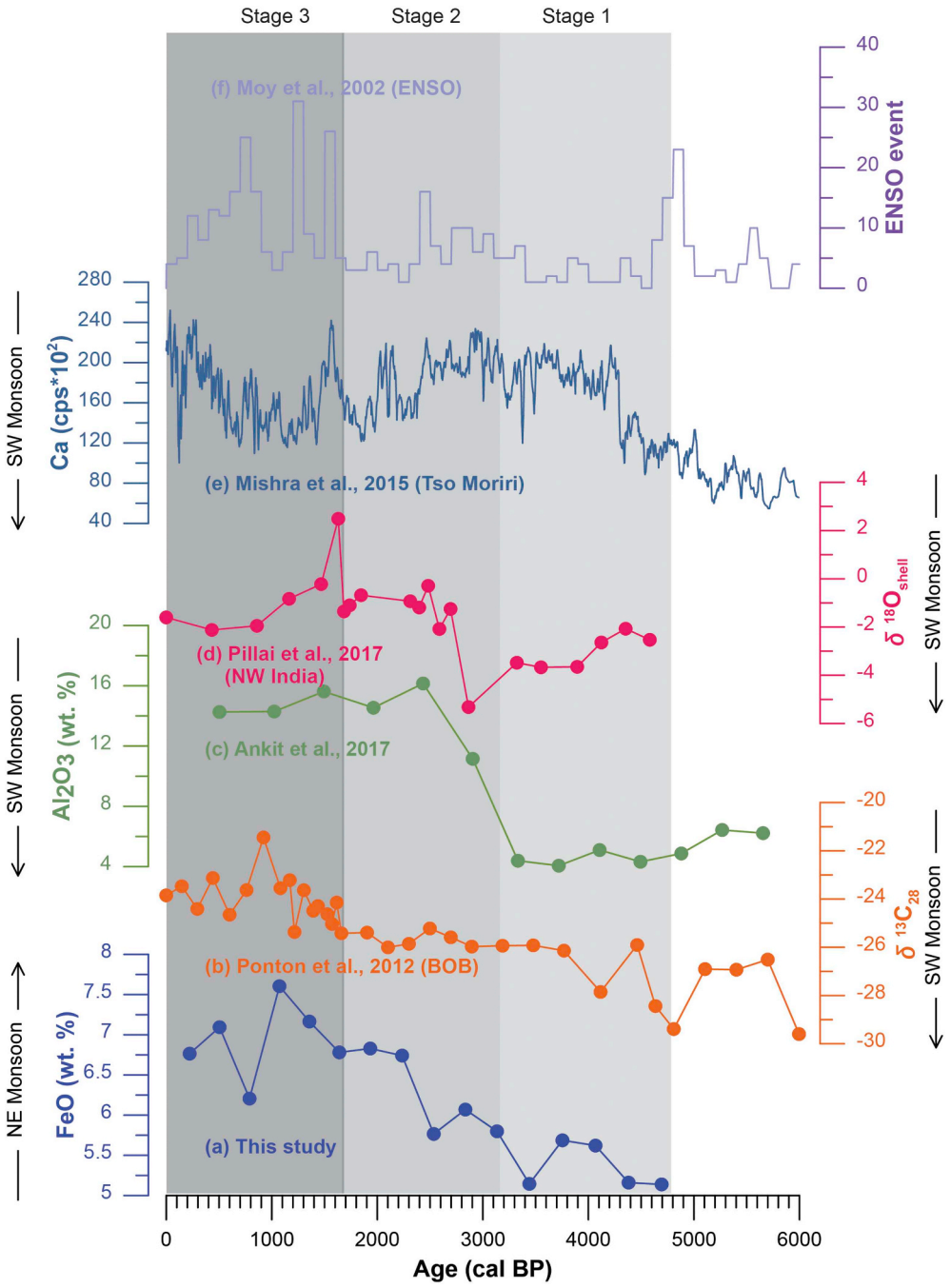

Fig. 5. Regional comparison of the paleoclimate data. Stage 1 to 3 is marked by shades of grey. For the locations discussed in the figure (a–e), please refer Fig. 1.

6. Conclusions

In this study, integrated geochemical and clay mineralogical analyses coupled with end member mixing analysis derived from grain size parameters are utilized to understand mid-late Holocene climate variability from Ennamangalam Lake, southern India. The multiproxy investigations revealed a progressive increase in precipitation through the identification of three hydrological stages: stage 1 (ca. 4800 to 3150 cal BP)-marked by relative drier condition with low detrital input and sedimentation rate and higher contribution of EM 2 (represents fine silt fraction); stage 2 (ca. 3150 to 1640 cal BP) is characterized by transition phase with high sedimentation rate as compared to the preceding stage; and stage 3 (1640 cal BP to present) represented by highest detrital content and dominance of EM 1 indicating high energy condition in the surface runoff due to enhanced precipitation in the region.

The regional comparison of paleoclimate data demonstrates an inverse relation between Ennamangalam records with the paleo-records from ISM precipitation affected regions. The gradual increasing moisture from ~4800 cal BP to present indicates the enhanced NE monsoon contribution in the study area during the late Holocene.

Acknowledgment

PKM (DST/INSPIRE/04/2015/002769) and AA (DST/INSPIRE/04/2015/001199) gratefully acknowledge the financial support provided by DST-INSPIRE faculty programme. We thank Dr. Birgit Gaye and Dr. R. Krishnan for useful discussions. A special thanks to Ms. Shweta Singh for help with the laboratory analysis. The authors confirm that they have no conflict of interest.

Appendix A. Supplementary data

Supplementary data to this article can be found online at https://doi.org/10.1016/j.catena.2019.104117.

References

Alizai, A., Hillier, S., Clift, P.D., Giosan, L., Hurst, A., VanLaningham, S., Macklin, M., 2012. Clay mineral variations in Holocene terrestrial sediments from the Indus Basin. Quat. Res. 77, 368–381. https://doi.org/10.1016/j.yqres.2012.01.008.

Ankit, Y., Kumar, P., Anoop, A., Mishra, P.K., Varghese, S., 2017. Mid-late Holocene climate variability in the Indian monsoon: evidence from continental shelf sediments adjacent to Rushikulya river, eastern India. Quat. Int. 443, 155–163.

Anoop, A., Prasad, S., Krishnan, R., Naumann, R., Dulski, P., 2013a. Intensified monsoon and spatiotemporal changes in precipitation patterns in the NW Himalaya during the early-mid Holocene. Quat. Int. 313–314, 74–84. https://doi.org/10.1016/j.quaint.2013.08.014.

Anoop, A., Prasad, S., Plessen, B., Basavaiah, N., Gaye, B., Naumann, R., Menzel, P., Weise, S., Brauer, A., 2013b. Palaeoenvironmental implications of evaporative gaylussite crystals from Lonar Lake, central India. J. Quat. Sci. 28, 349–359. https://doi.org/10.1002/jqs.2625.

Banerji, U.S., Pandey, S., Bhushan, R., Juyal, N., 2015. Mid-Holocene climate and land-sea interaction along the southern coast of Saurashtra, western India. J. Asian Earth Sci. 111, 428–439. https://doi.org/10.1016/j.jseaes.2015.06.021.

Basavaiah, N., Wiesner, M.G., Anoop, A., Menzel, P., Nowaczyk, N.R., Deenadayalan, K., Brauer, A., Gaye, B., Naumann, R., Riedel, N., Prasad, M.S.S., 2014. Physicochemical analyses of surface sediments from the Lonar Lake, central India – implications for palaeoenvironmental reconstruction. Fundam. Appl. Limnol. / Arch. für Hydrobiol. 184, 51–68. https://doi.org/10.1127/1863-9135/2014/0515.

Basu, S., Anoop, A., Sanyal, P., Singh, P., 2017. Lipid distribution in the lake Ennamangalam, south India: indicators of organic matter sources and paleoclimatic history. Quat. Int. 443, 238–247. https://doi.org/10.1016/j.quaint.2016.08.045.

Beuscher, S., Kru, S., Ehrmann, W., Schmiedl, G., Milker, Y., Arz, H., Schulz, H., 2017. End-member modelling as a tool for climate reconstruction — an Eastern Mediterranean case study. PLoS One 12, 1–22.

Bhattacharya, T., Byrne, R., 2016. Cultural implications of late Holocene climate change in the Cuenca Oriental, Mexico. Proc. Natl. Acad. Sci. 112, 56–69.

Biscaye, P.E., 1965. Mineralogy and sedimentation of recent deep-sea clay in the Atlantic Ocean and adjacent seas and oceans. Geol. Soc. Am. Bull. 76, 803–832.

Borchers, A., Dietze, E., Kuhn, G., Esper, O., Voigt, I., Hartmann, K., Diekmann, B., 2016. Holocene ice dynamics and bottom-water formation associated with Cape Darnley polynya activity recorded in Burton Basin, East Antarctica. Mar. Geophys. Res. 37, 49–70. https://doi.org/10.1007/s11001-015-9254-z.

Breitenbach, S.F.M., Adkins, J.F., Meyer, H., Marwan, N., Kumar, K.K., Haug, G.H., 2010. Strong influence of water vapor source dynamics on stable isotopes in precipitation observed in Southern Meghalaya, NE India. Earth Planet. Sci. Lett. 292, 212–220. https://doi.org/10.1016/j.epsl.2010.01.038.

Brown, G., Brindley, G.Wi, 1980. Crystal Structures of Clay Minerals and Their X-ray Identification. Mineralogical Society London.

Buggle, B., Glaser, B., Hambach, U., Gerasimenko, N., Marković, S., 2011. An evaluation of geochemical weathering indices in loess–paleosol studies. Quat. Int. 240, 12–21. https://doi.org/10.1016/j.quaint.2010.07.019.

Churchman, G.J., 2000. The alteration and formation of soil minerals by weathering. Handb. soil Sci. 3–76.

Cuven, S., Francus, P., Lamoureux, S.F., 2010. Estimation of grain size variability with micro X-ray fluorescence in laminated lacustrine sediments, Cape Bounty, Canadian High Arctic. J. Paleolimnol. 44, 803–817. https://doi.org/10.1007/s10933-010-9453-1.

Demske, D., Tarasov, P.E., Wünnemann, B., Riedel, F., 2009. Late glacial and Holocene vegetation, Indian monsoon and westerly circulation in the Trans-Himalaya recorded in the lacustrine pollen sequence from Tso Kar, Ladakh, NW India. Palaeogeogr. Palaeoclimatol. Palaeoecol. 279, 172–185. https://doi.org/10.1016/j.palaeo.2009.05.008.

Dhar, O.N., Rakhecha, P.R., 1983. Foreshadowing northeast monsoon rainfall over Tamil Nadu, India. Am. Meteorol. Soc. 111, 109–111.

Dietze, E., Hartmann, K., Diekmann, B., IJmker, J., Lehmkuhl, F., Opitz, S., Stauch, G., Wünnemann, B., Borchers, A., 2012. An end-member algorithm for deciphering modern detrital processes from lake sediments of Lake Donggi Cona, NE Tibetan Plateau, China. Sediment. Geol. 243–244, 169–180. https://doi.org/10.1016/j.sedgeo.2011.09.014.

Dietze, E., Wünnemann, B., Hartmann, K., Diekmann, B., Jin, H., Stauch, G., Yang, S., Lehmkuhl, F., 2013. Early to mid-Holocene lake high-stand sediments at Lake Donggi Cona, northeastern Tibetan Plateau, China. Quat. Res. 79, 325–336. https://doi.org/10.1016/j.yqres.2012.12.008.

Dietze, E., Maussion, F., Ahlborn, M., Diekmann, B., Hartmann, K., Henkel, K., Kasper, T., Lockot, G., Opitz, S., Haberzettl, T., 2014. Sediment transport processes across the Tibetan Plateau inferred from robust grain-size end members in lake sediments. Clim. Past 10, 91–106. https://doi.org/10.5194/cp-10-91-2014.

El-nady, M.M., Lotfy, N.M., 2016. Multivariate geochemical and statistical methods applied to assessment of organic matter potentiality and its correlation with hydrocarbon maturity parameters (case study: Safir-1x well, North Western Desert, Egypt). Egypt. J. Pet. 25, 555–563. https://doi.org/10.1016/j.ejpe.2015.12.001.

Engstrom, D.R., Wright, W.E.J., 1984. Chemical stratigraphy of lake sediments as a record of environmental change. In: Lake Sediments and Environmental History: Studies in Palaeolimnology and Palaeoecology in Honour of Winifred Tutin.

Fagel, N., Boës, X., 2008. Clay-mineral record in Lake Baikal sediments: the Holocene and Late Glacial transition. Palaeogeogr. Palaeoclimatol. Palaeoecol. 259, 230–243. https://doi.org/10.1016/j.palaeo.2007.10.009.

Fedo, C.M., Nesbitt, H.W., Young, G.M., 1995. Unraveling the effects of potassium metasomatism in sedimentary rocks and paleosols, with implications for paleoweathering conditions and provenance. Geology 23, 921–924.

Gadgil, S., 2006. The Indian monsoon. Resonance 11, 8–21. https://doi.org/10.1007/BF02834470.

Galán, E., 2016. Chapter 14 genesis of clay minerals. In: Bergaya, F., Theng, B.K.G., Lagaly, G. (Eds.), Handbook of Clay Science, https://doi.org/10.1016/S1572-4352(05)01042-1.

Gaye, B., Böll, A., Segschneider, J., Burdanowitz, N., Emeis, K.C., Ramaswamy, V., Lahajnar, N., Lückage, A., Rixen, T., 2017. Glacial-interglacial changes and Holocene variations in Arabian Sea denitrification. Biogeosci. Discuss. 1–41.

George, G., Charlotte, B.V., Ruchith, R.D., 2011. Interannual variation of northeast monsoon rainfall over southern peninsular India. Indian J. Mar. Sci. 40, 98–104.

Gioia, D., Leo, P., Giano, S.I., Schiattarella, M., 2011. Chronological constraints on a holocene landslide in an intermontane basin of the southern Apennines, Italy: morphological evolution and palaeoclimate implications. Holocene 21, 263–273. https://doi.org/10.1177/0959683610378879.

Girone, A., Capotondi, L., Ciaranfi, N., Di Leo, P., Lirer, F., Maiorano, P., Marino, M., Pelosi, N., Pulice, I., 2013. Paleoenvironmental changes at the lower Pleistocene Montalbano Jonico section (southern Italy): global versus regional signals. Palaeogeogr. Palaeoclimatol. Palaeoecol. 371, 62–79. https://doi.org/10.1016/j.palaeo.2012.12.017.

Gunnell, Y., Anupama, K., Sultan, B., 2007. Response of the South Indian runoff-harvesting civilization to northeast monsoon rainfall variability during the last 2000 years: instrumental records and indirect evidence. The Holocene 17, 207–215.

Hamann, Y., Ehrmann, W., Schmiedl, G., Krüger, S., Stuut, J.-B., Kuhnt, T., 2008. Sedimentation processes in the Eastern Mediterranean Sea during the Late Glacial and Holocene revealed by end-member modelling of the terrigenous fraction in marine sediments. Mar. Geol. 248, 97–114.

Hardy, R., Tucker, M., 1988. X-ray powder diffraction of sediments. Tech. Sedimentol. 191–228.

Hofer, G., Wagreich, M., Neuhuber, S., 2013. Geochemistry of fine-grained sediments of the upper Cretaceous to Paleogene Gosau Group (Austria, Slovakia): implications for paleoenvironmental and provenance studies. Geosci. Front. 4, 449–468. https://doi.org/10.1016/j.gsf.2012.11.009.

Hou, J., Andrea, W.J.D., Liu, Z., 2012. The influence of 14C reservoir age on interpretation of paleolimnological records from the Tibetan Plateau. Quat. Sci. Rev. 48, 67–79.

Issaka, S., Ashraf, M.A., 2017. Impact of soil erosion and degradation on water quality: a review. Geol. Ecol. Landscapes 9508, 1–11. https://doi.org/10.1080/24749508.2017.1301053.

Kavidha, R., Elangovan, K., 2012. Assessment of groundwater potential zones in Erode District, Tamil Nadu, by using GIS techniques. Pollut. Res. 31, 31–37.

Keller, W.D., 1970. Environmental aspects of clay minerals. J. Sediment. Res. 40, 788–854.

Koinig, K.A., Shotyk, W., Ohlendorf, C., Sturm, M., 2003. 9000 Years of Geochemical Evolution of Lithogenic Major and Trace Elements in the Sediment of an Alpine Lake – The Role of Climate, Vegetation, and Land-4. pp. 307–320.

Kripalani, R.H., Kumar, P., 2004. Northeast monsoon rainfall variability over south peninsular India vis-à-vis the Indian Ocean dipole mode. Int. J. Climatol. 24, 1267–1282. https://doi.org/10.1002/joc.1071.

Krishna Kumar, K., Rupa Kumar, K., Ashrit, R.G., Deshpande, N.R., Hansen, J.W., 2004. Climate impacts on Indian agriculture. Int. J. Climatol. 24, 1375–1393. https://doi.org/10.1002/joc.1081.

Laskar, A.H., Yadava, M.G., Sharma, N., Ramesh, R., 2013. Late-Holocene climate in the Lower Narmada valley, Gujarat, western India, inferred using sedimentary carbon and oxygen isotope ratios. The Holocene 23, 1115–1122.

Leipe, C., Demske, D., Tarasov, P.E., Wünnemann, B., Riedel, F., 2014. Potential of pollen and non-pollen palynomorph records from Tso Moriri (Trans-Himalaya, NW India) for reconstructing Holocene limnology and human–environmental interactions. Quat. Int. 348, 113–129. https://doi.org/10.1016/j.quaint.2014.02.026.

Leng, M.J., Jones, M.D., Frogley, M.R., Eastwood, W.J., Kendrick, C.P., Roberts, C.N., 2010. Detrital carbonate influences on bulk oxygen and carbon isotope composition of lacustrine sediments from the Mediterranean. Glob. Planet. Change 71, 175–182. https://doi.org/10.1016/j.gloplacha.2009.05.005.

Li, T., Li, T., 2017. Sediment transport processes in the Pearl River Estuary as revealed by grain-size end-member modeling and sediment trend analysis. Geo-Marine Lett 1–12. https://doi.org/10.1007/s00367-017-0518-2.

Limmer, D.R., Böning, P., Giosan, L., Ponton, C., Köhler, C.M., Cooper, M.J., Tabrez, A.R., Clift, P.D., 2012. Geochemical record of Holocene to Recent sedimentation on the Western Indus continental shelf, Arabian Sea. Geochemistry, Geophys. Geosystems 13, 1–26. https://doi.org/10.1029/2011GC003845.

Liu, Z., Colin, C., Huang, W., Le, K.P., Tong, S., Chen, Z., Trentesaux, A., 2007. Climatic and tectonic controls on weathering in south China and Indochina Peninsula: clay mineralogical and geochemical investigations from the Pearl, Red, and Mekong drainage basins. Geochemistry, Geophys. Geosystems 8.

Lopez, P., Navarro, E., Marce, R., Ordoñez, J., Caputo, L., Armengol, J., 2006. Elemental ratios in sediments as indicators of ecological processes in Spanish reservoirs. Limnetica 25, 499–512. https://doi.org/10.1144/GSL.SP.2006.267.01.06.

McLennan, S.M., Henning, S., McDaniel, D.K., Hanson, G.N., 1993. Geochemical approaches to sedimentation, provenance, and tectonics. Geol. Soc. Am. 21–39.

Miesch, A.T., 1976. Q-mode factor analysis of compositional data. Comput. Geosci. 1, 147–159.

Minyuk, P.S., Borkhodoev, V.Y., Wennrich, V., 2013. Inorganic data from El'gygytgyn Lake sediments: stages 6–11. Clim. Past Discuss. 9, 393–433. https://doi.org/10.

5194/cpd-9-393-2013.
Mischke, S., Weynell, M., Zhang, C., Wiechert, U., 2013. Spatial variability of 14C reservoir effects in Tibetan Plateau lakes. Quat. Int. 313–314, 147–155. https://doi.org/10.1016/j.quaint.2013.01.030.
Mishra, P.K., Anoop, A., Schettler, G., Prasad, S., Jehangir, A., Menzel, P., Naumann, R., Yousuf, A, R., Basavaiah, N., Deenadayalan, K., Wiesner, M G., Gaye, B., 2015. Reconstructed late Quaternary hydrological changes from Lake Tso Moriri, NW Himalaya. Quat. Int. 371, 76–86. doi:https://doi.org/10.1016/j.quaint.2014.11.040.
Mishra, P.K., Prasad, S., Jehangir, A., Anoop, A., Yousuf, A.R., Gaye, B., 2018a. Investigating the role of meltwater versus precipitation seasonality in abrupt lake-level rise in the high-altitude Tso Moriri Lake (India). Palaeogeogr. Palaeoclimatol. Palaeoecol 493, 20–29. https://doi.org/10.1016/j.palaeo.2017.12.026.
Mishra, P.K., Prasad, S., Marwan, N., Anoop, A., Krishnan, R., Gaye, B., Basavaiah, N., Stebich, M., Menzel, P., Riedel, N., 2018b. Contrasting pattern of hydrological changes during the past two millennia from central and northern India: regional climate di ff erence or anthropogenic impact ? Glob 161, 97–107. https://doi.org/10.1016/j.gloplacha.2017.12.005.
Moy, C.M., Seltzer, G.O., Rodbell, D.T., Anderson, D.M., 2002. Variability of El Nino/Southern Oscillation activity at millennial timescales during the Holocene epoch. Nature 420, 162–165. https://doi.org/10.1038/nature01163.1.
Nagasundaram, M., Achyuthan, H., Ahmad, S.M., 2013. Monsoonal changes inferred from the Middle to Late Holocene sediments off Landfall Island, North Andaman. Arab. J. Geosci. 7, 3513–3523. https://doi.org/10.1007/s12517-013-1010-6.
Nanthakumar, K.K.K., Tamilarasi, P.V.S., Lakshmanaperumalsamy, P., 2010. Prevalence of Certain Inorganic Constituents in Groundwater Samples of Erode District, Tamilnadu, India, With Special Emphasis on Fluoride, Fluorosis and Its Remedial Measures. pp. 141–155. https://doi.org/10.1007/s10661-008-0664-0.
Nesbitt, H.W., Young, G.M., 1989. Formation and diagenesis of weathering profiles. J. Geol. 97, 129–147.
Odoma, A.N., Obaje, N.G., Idakwo, S.O., Erbacher, J., 2013. Paleoclimate reconstruction during Mamu Formation (Cretaceous) based on clay mineral distributions. IOSR J. Appl. Geol. Geophys. 1, 40–46.
Opitz, S., Zhang, C., Herzschuh, U., Mischke, S., 2015. Climate variability on the south-eastern Tibetan Plateau since the Lateglacial based on a multiproxy approach from Lake Naleng – comparing pollen and non-pollen signals. Quat. Sci. Rev. 115, 112–122. https://doi.org/10.1016/j.quascirev.2015.03.011.
Peucat, J.J., Vidal, P., Bernard-Griffiths, J., Condie, K.C., 1989. Sr, Nd, and Pb isotopic systematics in the Archean low- to high-grade transition zone of southern India: syn-accretion vs. post-accretion granulites. J. Geol. 97, 537–549. https://doi.org/10.1086/629333.
Pillai, A.A.S., Anoop, A., Sankaran, M., Sanyal, P., Jha, D.K., Ratnam, J., 2017. Mid-late Holocene vegetation response to climatic drivers and biotic disturbances in the Banni grasslands of western India. Palaeogeogr. Palaeoclimatol. Palaeoecol. 485, 869–878.
Ponton, C., Giosan, L., Eglinton, T.I., Fuller, D.Q., Johnson, J.E., Kumar, P., Collett, T.S., 2012. Holocene aridification of India. Geophys. Res. Lett. 39, 1–6. https://doi.org/10.1029/2011GL050722.
Prasad, S., Enzel, Y., 2006. Holocene paleoclimates of India. Quat. Res. 66, 442–453. https://doi.org/10.1016/j.yqres.2006.05.008.
Prasad, S., Anoop, A., Riedel, N., Sarkar, S., Menzel, P., Basavaiah, N., Krishnan, R., Fuller, D., Plessen, B., Gaye, B., Röhl, U., Wilkes, H., Sachse, D., Sawant, R., Wiesner, M.G., Stebich, M., 2014. Prolonged monsoon droughts and links to Indo-Pacific warm pool: a Holocene record from Lonar Lake, central India. Earth Planet. Sci. Lett. 391, 171–182. https://doi.org/10.1016/j.epsl.2014.01.043.
Pulice, I., Di Leo, P., Robustelli, G., Scarciglia, F., Cavalcante, F., Belviso, C., 2013. Control of climate and local topography on dynamic evolution of badland from southern Italy (Calabria). Catena 109, 83–95. https://doi.org/10.1016/j.catena.2013.05.001.
Railsback, B., 1993. A geochemical view of weathering and the origin of sedimentary rocks and natural waters. J. Geol. Educ. 41, 404–411.
Rajeevan, M., Gadgil, S., Bhate, J., 2010. Active and break spells of the indian summer monsoon. J. Earth Syst. Sci. 119, 229–247. https://doi.org/10.1007/s12040-010-0019-4.
Rajeevan, M., Unnikrishnan, C.K., Bhate, J., Niranjan Kumar, K., Sreekala, P.P., 2012. Northeast monsoon over India: variability and prediction. Meteorol. Appl. 19, 226–236. https://doi.org/10.1002/met.1322.
Rajkumar, N., Subramani, T., Elango, L., 2010. Groundwater contamination due to municipal solid waste disposal – a GIS based study in Erode City. Int. J. Environ. Sci. 1, 39–55.
Rajmanickam, V., Achyuthan, H., Eastoe, C., Farooqui, A., 2017. Early-Holocene to present palaeoenvironmental shifts and short climate events from the tropical wetland and lake sediments, Kukkal Lake, Southern India: geochemistry and palynology. Holocene 27, 404–417. https://doi.org/10.1177/0959683616660162.
Ramsey, C.B., Dee, M., Lee, S., Nakagawa, T., Staff, R.A., 2010. Developments in the calibration and modelling of radiocarbon dates. Radiocarbon 52, 953–961.
Ranasinghe, P., Ortiz, J., Smith, A., Griffith, E., Siriwardana, C., De Silva, S., Wijesundara, D., 2013. Mid- to late-Holocene Indian winter monsoon variability from a terrestrial record in eastern and southeastern coastal environments of Sri Lanka. The Holocene 23, 945–960. https://doi.org/10.1177/0959683612475141.
Rao Krishna, P.R., Jagannathan, P., 1953. A study of the northeast monsoon rainfall of Tamilnadu. Indian J. Meteorol. Geophys. 4, 22–43.
Rawat, S., Gupta, A.K., Sangode, S.J., Srivastava, P., Nainwal, H.C., 2015. Late Pleistocene–Holocene vegetation and Indian summer monsoon record from the Lahaul, Northwest Himalaya, India. Quat. Sci. Rev. 114, 167–181. https://doi.org/10.1016/j.quascirev.2015.01.032.
Ray, L., Kumar, P.S., Reddy, G.K., Roy, S., Rao, G.V., Srinivasan, R., Rao, R.U.M., 2003. High mantle heat flow in a Precambrian granulite province: evidence from southern India. J. Geophys. Res. Solid Earth 108, 6/1–6/13. https://doi.org/10.1029/2001JB000688.
Reimer, P.J., Bard, E., Bayliss, A., Beck, J.W., Blackwell, P.G., Ramsey, C.B., 2013. IntCal13 and Marine13 radiocarbon age calibration curves 0–50,000 years cal BP. Radiocarbon 55, 1869–1887. https://doi.org/10.2458/azu_js_rc.55.16947.
Samuel, V.O., Kwon, S., Santosh, M., Sajeev, K., 2018. Garnet pyroxenite from Nilgiri Block, southern India: vestiges of a Neoarchean volcanic arc. LITHOS 310–311, 120–135. https://doi.org/10.1016/j.lithos.2018.04.009.
Sandeep, K., Shankar, R., Warrier, A.K., Yadava, M.G., Ramesh, R., Jani, R.A., Weijian, Z., Xuefeng, L., 2017. A multi-proxy lake sediment record of Indian summer monsoon variability during the Holocene in southern India. Palaeogeogr. Palaeoclimatol. Palaeoecol. 476, 1–14. https://doi.org/10.1016/j.palaeo.2017.03.021.
Sanwal, J., Kotlia, B.S., Rajendran, C., Ahmad, S.M., Rajendran, K., Sandiford, M., 2013. Climatic variability in Central Indian Himalaya during the last ~1800 years: evidence from a high resolution speleothem record. Quat. Int. 304, 183–192. https://doi.org/10.1016/j.quaint.2013.03.029.
Sarkar, S., Prasad, S., Wilkes, H., Riedel, N., Stebich, M., Basavaiah, N., Sachse, D., 2015. Monsoon source shifts during the drying mid-Holocene: biomarker isotope based evidence from the core “monsoon zone” (CMZ) of India. Quat. Sci. Rev. 123, 144–157. https://doi.org/10.1016/j.quascirev.2015.06.020.
Shapiro, L.M., Brannock, W.W., 1962. Rapid Analysis of Silicate, Carbonate and Phosphate Rocks. US Government Printing Office.
Shetty, S.B., Shankar, R., Weijian, Z., Peng, C., 2018. Magnetic susceptibility as a proxy for rainfall in the tropics: new data from Hirekolale Lake sediments, southern India. Int. J. Sci. Res. Sci. Technol. 4, 1354–1369.
Singer, A., 1980. The paleoclimatic interpretation of clay minerals in soils and weathering profiles. Earth-Science Rev 15, 303–326. https://doi.org/10.1016/0012-8252(80)90113-0.
Sinha, A., Kathayat, G., Cheng, H., Breitenbach, S.F.M., Berkelhammer, M., Mudelsee, M., Biswas, J., Edwards, R.L., 2015. Trends and oscillations in the Indian summer monsoon rainfall over the last two millennia. Nat. Commun. 6, 7309.
Sreekala, P.P., Rao, S.V.B., Rajeevan, M., 2012. Northeast monsoon rainfall variability over south peninsular India and its teleconnections. Theor. Appl. Climatol. 108, 73–83. https://doi.org/10.1007/s00704-011-0513-x.
Srivastava, P., Agnihotri, R., Sharma, D., Meena, N., Sundriyal, Y.P., Saxena, A., Bhushan, R., Sawlani, R., Banerji, U.S., Sharma, C., Bisht, P., Rana, N., Jayangondaperumal, R., 2017. 8000-year monsoonal record from Himalaya revealing reinforcement of tropical and global climate systems since mid-Holocene. Sci. Rep. 7, 1–11. https://doi.org/10.1038/s41598-017-15143-9.
Środoń, J., 1999. Use of Clay Minerals in Reconstructing Geological Processes: Recent Advances and Some Perspectives. vol. 34. pp. 27–37.
Sukumar, R., Ramesh, R., Pant, R.K., Rajagopalan, G., 1993. A δ13C record of late Quaternary climate change from tropical peats in southern India. Nature 364, 703.
Talbot, M.R., 1990. A review of the palaeohydrological interpretation of carbon and oxygen isotopic ratios in primary lacustrine carbonates. Chem. Geol. Isot. Geosci. Sect. 80, 261–279. https://doi.org/10.1016/0168-9622(90)90009-2.
Thamban, M., Purnachandra Rao, V., Schneider, R., 2002. Reconstruction of late Quaternary monsoon oscillations based on clay mineral proxies using sediment cores from the western margin of India. Mar. Geol. 186, 527–539. https://doi.org/10.1016/S0025-3227(02)00268-2.
Vandenberghe, J., Zhisheng, A., Nugteren, G., Huayu, L., Van Huissteden, K., 1997. New absolute time scale for the Quaternary climate in the Chinese Loess region by grain-size analysis. Geology 25, 35–38.
Veena, M.P., Achyuthan, H., Eastoe, C., Farooqui, A., 2014. A multi-proxy reconstruction of monsoon variability in the late Holocene, South India. Quat. Int. 325, 63–73. https://doi.org/10.1016/j.quaint.2013.10.026.
Weltje, G.J., 1997. End-member modeling of compositional data: numerical-statistical algorithms for solving the explicit mixing problem. Math. Geol. 29, 503–549. https://doi.org/10.1007/BF02775085.
Wünnemann, B., Demske, D., Tarasov, P., Kotlia, B.S., Reinhardt, C., Bloemendal, J., Diekmann, B., Hartmann, K., Krois, J., Riedel, F., 2010. Hydrological evolution during the last 15kyr in the Tso Kar lake basin (Ladakh, India), derived from geomorphological, sedimentological and palynological records. Quat. Sci. Rev. 29, 1138–1155. https://doi.org/10.1016/j.quascirev.2010.02.017.
Xue, J., Lee, C., Wakeham, S.G., Armstrong, R.A., 2011. Using principal components analysis (PCA) with cluster analysis to study the organic geochemistry of sinking particles in the ocean. Org. Geochem. 42, 356–367. https://doi.org/10.1016/j.orggeochem.2011.01.012.
Yadav, R.K., 2012. Why is ENSO influencing Indian northeast monsoon in the recent decades? Int. J. Climatol. 32, 2163–2180. https://doi.org/10.1002/joc.2430.
Yuretich, R., Melles, M., Sarata, B., Grobe, H., 1999. Clay minerals in the sediments of Lake Baikal: a useful climate proxy. J. Sediment. Res. 69, 588–596. https://doi.org/10.2110/jsr.69.588.
Zhong, W., Pen, Z., Xue, J., Ouyang, J., Tang, X., Cao, J., 2012. Geochemistry of sediments from Barkol Lake in the westerly influenced northeast Xinjiang: implications for catchment weathering intensity during the Holocene. J. Asian Earth Sci. 50, 7–13.